Human intervertebral disc stiffness correlates better with the Otsu threshold computed from axial T_2 map of its posterior annulus fibrosus than with clinical classifications

Ghislain Maquer [1], Vaclav Brandejsky [2], Lorin M. Benneker [3], Atsuya Watanabe [4], Peter Vermathen [2] and Philippe K. Zysset [1*]

[1] Institute of Surgical Technology and Biomechanics, University of Berne, Switzerland

[2] Department of Clinical Research, University of Berne, Switzerland

[3] Department of Orthopaedic Surgery, Inselspital, University of Berne, Switzerland

[4] Department of Orthopaedic Surgery, Teikyo University, Ichihara, Japan

*Corresponding author: Philippe K. Zysset, Ph.D.

Institute of Surgical Technology and Biomechanics, University of Bern

Stauffacherstrasse 78, CH-3014 Bern

Tel: +41 31 631 59 25

Fax: +41 31 631 59 60

E-mail: philippe.zysset@istb.unibe.ch

Keywords: Human intervertebral disc, Experimental stiffness, Degeneration grade, MRI, Axial T_2 maps

Number of words: 3138

Words abstract: 212

Number of figures: 3

Number of tables: 2 + 1 in supplementary data

Abstract

Degeneration of the intervertebral disc, sometimes associated with low back pain and abnormal spinal motions, represents a major health issue with high costs. A non-invasive degeneration assessment via qualitative or quantitative MRI (magnetic resonance imaging) is possible, yet, no relation between mechanical properties and T_2 maps of the intervertebral disc (IVD) has been considered, albeit T_2 relaxation time values quantify the degree of degeneration. Therefore, MRI scans and mechanical tests were performed on 14 human lumbar intervertebral segments freed from posterior elements and all soft tissues excluding the IVD. Degeneration was evaluated in each specimen using morphological criteria, qualitative T_2 weighted images and quantitative axial T_2 map data and stiffness was calculated from the load-deflection curves of *in vitro* compression, torsion, lateral bending and flexion/extension tests. In addition to mean T_2, the OTSU threshold of T_2 (T_{OTSU}), a robust and automatic histogram-based method that computes the optimal threshold maximizing the distinction of two classes of values, was calculated for anterior, posterior, left and right regions of each annulus fibrosus (AF). While mean T_2 and degeneration schemes were not related to the IVDs' mechanical properties, T_{OTSU} computed in the posterior AF correlated significantly with those classifications as well as with all stiffness values. T_{OTSU} should therefore be included in future degeneration grading schemes.

1. Introduction

Low back pain affects at least half of the western population and is responsible for high health care expenses every year [1]. Its origin is multifactorial. In cases of mechanical failure, degeneration of the intervertebral disc (IVD) is the initiating event and is associated with high risk of prolapse and herniation [2]. The intervertebral disc, composed of the fibrous annulus fibrosus and the gelatinous nucleus pulposus, ensures mobility of the segments and contributes to spinal stability [3, 4]. As degeneration occurs, the pressure in the dehydrated nucleus decreases, the disc height reduces and the collagen structure is modified, eventually leading to initiation of lesions and protrusions in the annulus due to abnormal load distribution on the endplates [5]. The stability of the segment is then affected by consequent alterations of the neutral zone [1], range of motion [6] and stiffness [7, 8].

Hence, efforts have been made to develop non-invasive methods for detection and evaluation of degeneration. Considering the influence of water content and collagen structure on T_1 and T_2 relaxation times, an assessment based on qualitative clinical MRI (magnetic resonance imaging) or quantitative MRI is possible [9-11]. Most morphological [12], $T_{1\rho}/T_2$-weighted [13] or T_2/T_2^* maps [2, 14] -based grading are performed on the sagittal plane of the intervertebral discs. Yet, some authors deem that T_2 maps acquired in the transverse plane are better suited for visualisation of posterolateral protrusions due to a larger field of view [9, 15].

The standard procedure consists of classifying the degeneration into discrete grades, which is unspecific and dependent on the operator's experience. The mechanical properties of a disc can hardly be related to its degenerative level because of the large standard deviations within each grade [6, 16, 17]. In addition, the impact of disc morphology on the biomechanical measurements is rarely considered [18-21].

In knee cartilage, a disorganised collagen structure with high water content is associated with high T_2 values [22] while negative correlations between T_2 value, compressive Young modulus and dynamic modulus were found [23-25]. Yet, no relation between mechanical properties and T_2 maps of the intervertebral disc has been considered despite the fact that T_1, T_2 and $T_{1\rho}$ values computed in the nucleus and annulus regions correlate with the degree of degeneration of the IVD [14], its radial and axial strains under compression [26, 27] as well as the compressive modulus and hydraulic permeability of the nucleus [28].

Clinicians visually evaluate the hydration of the nucleus based on intensity and homogeneity of the T_2 signal. To achieve equivalent evaluations quantitatively, the measure of T_2 at various locations [15, 14], entropy and geometry-based criteria [29] were recently proposed. Otsu is a robust method that computes the optimal threshold that maximizes the separability of two classes of values [30]. Being histogram-based and automatic, it produces an objective result unbiased by spatial information or by human interaction. Extensively used for the segmentation of the IVD [31-33], it also bears information about homogeneity. The Otsu threshold of a homogenous image is equal to its mean T_2 value but it will be biased by the intensity and frequency of high intensity pixels, which may be linked to the presence of annular tears [2].

Relying on the potential relation between quantitative T_2 maps and biochemical properties, the aim of this work is to propose a criterion for disc degeneration related to its mechanics and meeting the objectivity and simplicity requirements. The degeneration grades of 14 human lumbar intervertebral discs evaluated using MRI data and quantitative T_2 measures were compared to the specimens' stiffness in compression, torsion, lateral bending and flexion/extension.

2. Materials and methods

2.1. Qualitative and quantitative MRI imaging

Fourteen (14) spinal segments (T12-L1, L2-L3, L4-L5) were extracted from 6 human lumbar spines (age 63-89) after approval of the Ethics Committee of the Medical University of Vienna. All specimens were taken from individuals who voluntarily donated their bodies to the Center of Anatomy and Cell Biology of the Medical University of Vienna for postmortem studies by their last will. The posterior elements were sectioned at the pedicles and all soft tissues but the central intervertebral discs were removed. The endplates of the cranial and caudal vertebral bodies were embedded in a 10 mm-thick layer of PMMA (polymethylmethacrylate). The specimens, identified by a number between 1 and 14 (Fig2, Fig3, Table1, TableA1), were stored in sealed polyethylene bags at -20°C. Specimens were thawed at room temperature (20°C) the night before MRI imaging and placed in a custom-built container filled with 0.9% saline water to avoid drying of the specimen and to ensure sufficient loading of the RF coil. MRI scans were performed on a clinical 3T system (Verio, Siemens Healthcare, Germany) with a 15-channel knee coil. Anatomical T_1 (T_R/T_E = 999/13 ms) and T_2-weighted images (T_R/T_E = 4990/114 ms) in axial, coronal and sagittal planes were acquired in order to document all pathological conditions. 0.3 mm in-plane resolution was achieved for each of the 0.8 mm thick axial slices (128*256 mm^2 field of view (FOV), 384*768 matrix) and coronal/sagittal slices (3 mm thickness, 140*256 mm^2 FOV, 240*768 matrix).

For the axial T_2 mapping, a multi spin-echo sequence with 22 different echoes was chosen for its relatively short acquisition times. The sequence parameters were T_R = 3650 ms, first echo 12.5 ms and last echo 275 ms with steps of 12.5 ms, 106*199 mm^2 FOV and 204*384 matrix (0.5 mm resolution). Each T2 map was calculated by exponential curve fitting using a in-house script from a 3mm thick slice acquired in the centre of the disc using the anatomical data to position the imaging plane (Matlab, Mathworks, Natick, U.S.A.).

Prior to the scanning of the specimens, 14 T_2 maps were taken from a test sample while the water temperature in the container was increased from 9°C to 20°C to verify the influence of temperature on T_2. Then, to assess the stability and repeatability of the procedure, 2 sets of 6 T_2 maps were acquired on the test specimen every 30 minutes on two different days (D1, D2). Coefficient of variation ($CV = \frac{100 * SD}{Mean}$) and relative comparison of the mean T_2 value between D1 and D2 ($\Delta_{D1D2} = 100 * \frac{Mean_{D1} - Mean_{D2}}{Mean_{D1}}$) were evaluated for regions of interest in the nucleus and annulus.

Finally, the 14 samples were scanned. A whole imaging session lasted approximately 2.5 hours at controlled temperature (22°C) and the T_2 maps were acquired at the end of each session to limit the influence of temperature (Fig1.).

2.2. MRI-based morphological parameters

A method was introduced to compute the morphological parameters from the anatomical MRI images. First, semi-manual segmentation of the IVD was performed using ITKsnap [34] and the MRI-based morphological data were calculated from the segmented image:

$$CSA = \sum_{i}^{N} A_i \qquad V = \sum_{i}^{M} V_i \qquad H = \frac{V}{CSA}$$

$$I_{xx} = \sum_{i}^{N} (y_i - y_c)^2 \qquad I_{yy} = \sum_{i}^{N} (x_i - x_c)^2 \qquad J = I_{xx} + I_{yy} \qquad (1)$$

The resolution being known, the volume (V) of the disc was calculated by summing the volume of the segmented voxels V_i (M voxels per disc). A similar approach was performed on the cross-sectional area A_i of voxels of the cross-section of the disc (N voxels per cross-section) as well as to compute CSA, J, I_{xx} and I_{yy} using a Python script. To lighten the calculation of the moments of inertia, an in-plane rotation was applied to the segmented image to fit the disc's lateral and antero-posterior diameters to the x and y-axis of the coordinate system of the image. Special care was also taken to relate the moment of inertia calculation to the centroid (x_c, y_c) of its cross-section. Finally, the average height (H) of the specimen was determined from the ratio of V over CSA.

2.3. Apparent intervertebral moduli

To measure the stiffness of the samples, non-destructive quasi-static experiments were conducted after the scanning. The specimens were wrapped in 0.9% saline–soaked gauze, aligned along the axis of a servo-hydraulic device (MTS, Bionix, U.S.A.) and compressed 5 times up to 1000 N at constant loading rate (2000 N/min). Each compression was followed by a release and the displacement of the superior vertebral body was monitored. Then, axial torsion, bilateral bending and flexion/extension tests were conducted without pre-load by applying 5 cycles of pure moments (-5 to 5 Nm) to the PMMA layer of the superior vertebral body at constant displacement rate (0.8°/s) via a spinal loading simulator [35, 36]. The positions of X-shaped reflective markers (4 LEDs, resolution 0.1 mm) fixed to both PMMA layers were registered via motion capture (Optotrak3020, Northern Digital, Canada). The relative angular displacements of the vertebral bodies were then computed in Matlab (Mathworks, Natick, U.S.A.). Meanwhile, the moments applied on the superior vertebral body were measured with a 6-axis load cell (MC3A, AMTI, U.S.A.). Only the 5th loading-unloading cycle was kept for evaluation. Because of the irregular distribution of the data points, least square minimization of the residuals (Python, [37]) was utilised to fit exponential or double sigmoid functions on the load-deflection curves [38].

Stiffness (K, N/mm or Nmm/°) was determined from the fitted load-deflection data for all 4 biomechanical tests of each specimen as the ratio of the load over the displacement for the same deformation, a 3° angle or 15% strain, to include even the stiffest discs. Finally, normalisation of the stiffness was necessary to limit the influence of a disc's size on its mechanics and properly relate its stiffness to any degenerative alterations. Therefore, the apparent modulus (K^N, MPa) was calculated by normalising K by height (H, mm), area (CSA, mm^2), polar moment of inertia (J, mm^4) or area moment of inertia along the lateral (I_{xx}) or anteroposterior diameter (I_{yy}) computed from the voxels of the anatomical T_1-weighted images (Eq1.):

$$K_C^N = \frac{K_C * H}{CSA} \qquad K_T^N = \frac{K_T * H}{J} \qquad K_B^N = \frac{K_B * H}{I_{xx}} \qquad K_{F/E}^N = \frac{K_{F/E} * H}{I_{yy}} \qquad (2)$$

2.4. Link between degeneration grade, quantitative MRI data and apparent modulus

Two clinicians independently evaluated the degeneration of the specimens with the Thompson [12], Benneker [13] and Watanabe [9] grading systems using the anatomical images or the axial T_2 maps without any knowledge of their stiffness. The choice of these grading schemes was motivated by their intrinsic differences. The Pfirrmann system is probably the most common classification based on qualitative MRI but still highly oriented on the Thompson grading. Unlike Pfirrmann, the Thompson system is not based on MRI but on the morphological evaluation of macroscopic mid sagittal slices of the disc specimen. The Watanabe classification relies only on axial T_2-maps while the Benneker scheme employs an additive score based on radiographs, CT or MRI. It is more precise and, unlike Thompson and Pfirrmann, validated against biochemical parameters of degeneration. Moreover, both Watanabe and Benneker were compared to Pfirrmann and proved to be better suited to the detection of the early stages of degeneration. A consensus table was established (Table1).

The Otsu threshold (T_{OTSU}) was implemented in Python based on Otsu et al. [30]. Mean T_2, Δ ($Mean_{nucleus}$ - $Mean_{annulus}$) and T_{OTSU} were computed from each segmented T_2 map for the nucleus, the annulus and the anterior, posterior, left and right regions of the annulus to assess whether the regional T_2 values can discriminate the loading direction. Each AF region was determined by a 90° angle after an ellipse was automatically fitted to the IVD via a

Python script and assuming a surface ratio of 43% between nucleus and annulus only if the distinction was not clear [39, 40] (Fig1.). Finally, correlations between age, grading schemes, Mean T_2, T_{OTSU} of each region and apparent moduli were established for every loading mode.

3. Results

The influence of temperature, the stability and the repeatability of the T_2 maps were checked. Even though the test specimen was scanned for a large span of temperatures (from 9 to 20°C), the coefficient of variation (CV) for the T_2 maps of the intervertebral disc was less than 1.7%. At constant temperature, CV dropped to less than 1% and the difference between Day1 and Day2, Δ_{D1D2}, was less than 4%.

Grading, T_2 maps, Mean T_2 and T_{OTSU} for all disc regions and apparent moduli for the 14 specimens can be found in the supplementary data (TableA1). As the data is sorted along increasing Thompson grade, the broad range of apparent moduli associated to each grade is obvious.

Coefficients of determination (R^2) between age, grading, apparent moduli and T_2 were computed (Table2). The age of the donor could not be related to any of the grading schemes, apparent moduli or T_2 values. High correlations were found between the 3 grading schemes ($R^2 > 0.73$) but their relation with the mechanical properties was rather poor as only Thompson correlated significantly with K_C ($R^2 = 0.36$), K_T ($R^2 = 0.42$) and K_B ($R^2 = 0.32$). No link with mean T_2 in the nucleus and annulus and the grading parameter "classifications" was found but significant positive correlations were observed between the classifications and T_{OTSU} values computed in the annulus fibrosus and its posterior region (Fig2.).

Lateral bending moduli left or right were not linked to T_2 relaxation time computed in the left or right region of the annulus. The same observation was made between flexion/extension and mean T_2 of the anterior region. Interestingly, the highest correlations were established between T_{OTSU} computed in the posterior region and the apparent moduli K_T, K_B, K_E and K_F

(Fig3.). Finally, the apparent modulus in compression K_C could not be related to any T_2 values.

4. Discussion

The quantification of T_2 relaxation time is related to the biochemical properties of the intervertebral disc. This gives advanced MRI methods the potential to objectively evaluate disc degeneration [29]. Although the compressive Young modulus of the articular cartilage is connected to its mean T_2 value [25], no such connection has been established for human intervertebral discs.

Two experts evaluated the degeneration of our samples by using the Thompson, Benneker and Watanabe disc degeneration classifications. Their ratings were performed independently but the evaluations are in good agreement. Although the Thompson scale is solely based on morphology, Watanabe focuses on T2 map signal while Benneker examines both the T_2w signal and morphology, the grading schemes correlated well. These grading schemes are repeatable as they describe degeneration only based on morphology and, to some extent, biochemistry without apparent relation to the mechanical function. Correlation between these grading schemes speaks to their quality, however, lack of a link with the biomechanics of the disc in currently used schemes may affect their relevance. T_{OTSU} does include such a link and should therefore be included in future schemes. Mean T_2 relaxation time in the nucleus and annulus did not correlate with the degeneration grades. Published data [41, 42] corroborates our results regarding the annulus but contradicts those pertaining to the nucleus. Unlike those studies, our T_2 maps were performed on cadaver specimens, as opposed to being performed *in vivo*, and the *in vitro* conditions may have lowered the water and proteoglycan content in the nucleus [11]. This may also explain why the nuclear T_{OTSU} is not related to the degeneration grades. In any case, the nuclear mean T_2 and $T_{OTSU,}$ with only poor connection to the mechanical measurements, are not a satisfactory degeneration criterion.

T_2 is inversely sensitive to the collagen content and orientation of these fibres: regions with a denser collagen network, as in the annulus, are associated with lower T_2 relaxation time [43, 11] while annular tears, induced by the degeneration, have higher local T_2 values[2]. These High Intensity Zones (HIZ) inevitably increase the value of the annular T_{OTSU} explaining why it correlated positively and significantly with all 3 grading systems.

Interestingly, annular T_{OTSU} also correlates significantly with torsional and lateral bending stiffnesses but not with the compressive one. Michalek et al. [8] showed that a loss of pressurization of the nucleus is responsible for alterations in the compressive behaviour of the disc, while the behaviour in torsion is influenced by the presence of annular fibre disruptions. As the collagen fibres also drive the mechanical response of the intervertebral disc in flexion, lateral bending and flexion/extension, any annular disruptions decrease the intervertebral stiffness for those loading modes as well [44]. Those annular conditions, resulting in a higher T_{OTSU} explain the significant negative correlations obtained between annular T_{OTSU} and the bending or torsional stiffnesses. These findings corroborate previous observations suggesting that the presence of HIZ in the intervertebral disc is associated with reduction of the intervertebral stiffness [45].

There is no relation between T_{OTSU} in lateral regions of the annulus and lateral loading or between T_{OTSU} in the anterior annulus and flexion/extension. Conversely, T_{OTSU} of the posterior annulus provides interesting results. Not only did it correlate significantly with all the grading schemes but also with all bending stiffnesses, including flexion and extension. This result is coherent with our previous assumption that T_{OTSU} is sensitive to annular disruptions insofar as most HIZ, sometimes associated with low back pain, occur in the posterior annulus [46].

There are limitations to be aware of. Since the intervertebral compliance is dependent on the loading rate and the hydration of the disc, only quasi-static tests were conducted.

Additionally, various loading rates would only offset the stiffness measurements [47]. Another limitation was that the posterior elements and surrounding soft tissues, such as muscles and ligaments that are also responsible for the spinal stability were removed. Human material is difficult to obtain, thus the donors were few and the samples old which might explain why the age of the donors was unrelated to T_2 measurements, stiffness or degeneration grade [6, 29]. The specimens were kept frozen, and while a small number of freeze-thaw cycles seem not to affect the flexibility of human spinal segments [48, 49] and the fact that this is the standard storage method, freezing may potentially damage the tissue. Finally, only one axial T_2 map was acquired in the middle of each disc and some out of plane annular features may have been missed.

Most of those limitations are inherent to *in vitro* conditions and cadaver testing, but the stiffness measurements must be performed *in vitro* in a controlled environment to be reliable. Moreover, not only do countless *in vivo* MRI studies already exist, but also the link with mechanical properties, fundamental in the understanding of spinal instability, is rarely considered. This is one of the first studies to highlight the relation between quantitative MRI and stiffness of the intervertebral disc. The low but significant correlations between Otsu threshold, classification schemes and mechanical measures might be improved by performing a similar study on fresh animal material; however, this raises the problem of interspecies comparison as no large animal model for disc degeneration exists [50]. One last limitation lies in the fact that, although clinical protocols were performed in this study, a knee coil was used for the imaging to maximise the signal-to-noise ratio.

In conclusion, this study shows that the usual classification schemes cannot be related to the stiffness of cadaveric human intervertebral disc, unlike quantitative T_2 measurements (T_{OTSU}) computed in the posterior part of the annulus fibrosus. Although this fully automatic method requires further validation for *in vivo* imaging conditions, its simplicity, minimal human interaction and link with biomechanical properties makes it an attractive candidate for clinical assessment of disc degeneration.

Acknowledgments

The authors thank Alexander Bürki and Marc Laurent for their help regarding the mechanical tests, Urs Röhrer for producing the MRI-compatible container (Institute of Surgical Technology and Biomechanics, University of Bern, Switzerland) and Dr. Michael L. Pretterklieber for providing the specimens (Center of Anatomy and Cell Biology, Department of Applied Anatomy, Medical University of Vienna, Austria). Finally, we also would like to acknowledge Prof. Chris Boesch (Department of Clinical Research, Inselspital, University of Berne, Switzerland) for the interesting discussions regarding magnetic resonance imaging and Allison Clouthier for reading this manuscript. The project was made possible through funding obtained from the European Community, Grant Agreement n° PITN-GA-2009-238690-SPINEFX.

Declarations

Competing Interests

None declared

Please state any sources of funding for your research

The project was made possible through funding obtained from the European Community, Grant Agreement n° PITN-GA-2009-238690-SPINEFX.

Please state whether Ethical Approval was given, by whom and the relevant Judgement’s reference number

We received approval of the Ethics Committee of the Medical University of Vienna. All specimens were taken from individuals who voluntarily donated their bodies to the Center of Anatomy and Cell Biology of the Medical University of

Vienna for postmortem studies by their last will. Reference EK Nr: 732/2010

References

[1] Panjabi M. Clinical spinal instability and low back pain. Journal of Electromyography and Kinesiology 2003;13:371–379.

[2] Trattnig S, Stelzeneder D, Goed S, Reissegger M, Mamisch TC, Paternostro-Sluga T, Weber M, Szomolanyi P, Welsch GH. Lumbar intervertebral disc abnormalities: comparison of quantitative T2 mapping with conventional MR at 3.0T. Eur Radiol 2010;20:2715–2722.

[3] Kirkaldy-Willis WH and Farfan HF. Instability of the lumbar spine. Clin Orthop Relat Res 1982;165:110–123.

[4] Stokes IA, Frymoyer JW. Segmental motion and instability. Spine 1987;12:688–691.

[5] Dolan P and Adams MA. Recent advances in lumbar spinal mechanics and their significance for modelling. Clin Biomech 2001;16-Suppl 1:S8-S16.

[6] Tanaka N, An HS, Lim T, Fujiwara A, Jeon C, Haughton VM. The relationship between disc degeneration and flexibility of the lumbar spine. The Spine Journal 2001;1:47–56.

[7] Haughton VM, Lim TH. and An HS. Intervertebral disk appearance correlated with stiffness of lumbar spinal motion segments. AJNR Am J Neuroradiol 1999;20:1161-1165.

[8] Michalek AJ, Funabashi KL and Iatridis JC. Needle puncture injury of the rat intervertebral disc affects torsional and compressive biomechanics differently. EurSpineJ 2010;19:2110–2116.

[9] Watanabe A, Benneker LM, Boesch C, Watanabe T, Obata T, Anderson SE. Classification of intervertebral disk degeneration with axial T2 mapping. AJR 2007;189:936–942.

[10] Mwale F, Iatridis JC, Antoniou J Quantitative MRI as a diagnostic tool of intervertebral disc matrix composition and integrity. EurSpineJ 2008;17(4):S432–S440.

[11] Marinelli NL, Haughton VM, Munoz A and Anderson PA. T2 relaxation times of intervertebral disc tissue correlated with water content and proteoglycan content. Spine 2009;34(5):520 –524.

[12] Thompson JP, Pearce RH, Schechter MT, Adams ME, Tsang IK, Bishop PB. Preliminary evaluation of a scheme for grading the gross morphology of the human intervertebral disc. Spine 1990;15:411–415.

[13] Benneker LM, Heini PF, Anderson SE, Alini M, Ito K. Correlation of radiographic and MRI parameters to morphological and biochemical assessment of intervertebral disc degeneration. Eur Spine J 2005;14: 27–35.

[14] Stelzeneder D, Welsch GH, Kovács BK, Goed S, Paternostro-Sluga T, Vlychou M, Friedrich K, Mamisch TC and Trattnig S. Quantitative T2 evaluation at 3.0 T compared to morphological grading of the lumbar intervertebral disc: A standardized evaluation approach

in patients with low back pain. European Journal of Radiology 2012;81:324-330.

[15] Hoppe S, Quirbach S, Mamisch TC, Krause FG, Werlen S and Benneker LM. Axial T2* mapping in intervertebral discs: a new technique for assessment of intervertebral disc degeneration. Eur Radiol 2012;22:2013–2019.

[16] Krismer M, Haid C, Behensky H, Kapfinger P, Landauer F and Rachbauer F. Motion in lumbar functional spine units during side bending and axial rotation moments depending on the degree of Degeneration. Spine 2000;25:2020-2027.

[17] Kettler A, Rohlmann F, Ring C, Mack C and Wilke HJ. Do early stages of lumbar intervertebral disc degeneration really cause instability? Evaluation of an in vitro database. Eur Spine J 2011;20:578–584.

[18] Elliott DM and Sarver JJ. Young investigator award winner: validation of the mouse and rat disc as mechanical models of the human lumbar disc. Spine 2004;29:713–722.

[19] Campana S, de Guise JA, Rillardon L, Mitton D, Skalli W. Lumbar intervertebral disc mobility: effect of disc degradation and of geometry. Eur J Orthop Surg Traumatol 2007;17:533–541.

[20] Beckstein JC, Sen S, Schaer TP, Vresilovic EJ and Elliott DM. Comparison of animal discs used in disc research to human lumbar disc axial compression mechanics and glycosaminoglycan content. Spine 2008;33:E166–E173.

[21] Showalter BL, Beckstein JC, Martin JT, Beattie EE, Espinoza Orías AA, Schaer TP, Vresilovic EJ and Elliott DM. Comparison of animal discs used in disc research to human lumbar disc. Spine 2012;7:E900–E907.

[22] Nieminen MT, Rieppo J, Toyras J, Hakumaki JM, Silvennoinen J, Hyttinen MM, Helminen HJ and Jurvelin JS. T2 relaxation reveals spatial collagen architecture in articular cartilage: a comparative quantitative mri and polarized light microscopic study. Magnetic Resonance in Medicine 2001;46:487-493.

[23] Kurkijarvi JE, Nissi MJ, Kiviranta I, Jurvelin JS and Nieminen MT. Delayed gadolinium-enhanced mri of cartilage (dgemric) and t2 characteristics of human knee articular cartilage: topographical variation and relationships to mechanical properties. Magnetic Resonance in Medicine 2004;52:41-46.

[24] Nissi MJ, Rieppo J, Toyras J, Laasanen MS, Kiviranta I, Nieminen MT and Jurvelin JS. Estimation of mechanical properties of articular cartilage with MRI dGEMRIC, T2 and T1 imaging in different species with variable stages of maturation. OsteoArthritis and Cartilage 2007 15:1141-1148.

[25] Julkunen P, Korhonen RK, Nissi MJ and Jurvelin JS. Mechanical characterization of articular cartilage by combining magnetic resonance imaging and finite-element analysis-a potential functional imaging technique. Phys. Med. Biol 2008;53:2425–2438.

[26] O'Connell GD, Malhotra NR, Vresilovic EJ, Elliott DM, The effect of nucleotomy and the dependence on degeneration of human intervertebral disc strain in axial compression,

Spine 2011;36(21):1765-71.

[27] O'Connell GD, Vresilovic EJ, Elliott DM. Human intervertebral disc internal strain in compression: the effect of disc region, loading position, and degeneration. J Orthop Res. 2011;29(4):547-555.

[28] Périé D, Iatridis JC, Demers CN, Goswami T, Beaudoin G, Mwale F, Antoniou J. Assessment of compressive modulus, hydraulic permeability and matrix content of trypsin-treated nucleus pulposus using quantitative MRI. J Biomech. 2006;39(8):1392-400.

[29] Mayerhofer ME, Stelzeneder D, Bachbauer W, Welsch GH, Mamisch TC, Szczypinski P, Weber M, Peters N, Fruehwald-Pallamar J, Puchner S and Trattnig S. Quantitative analysis of lumbar intervertebral disc abnormalities at 3.0 Tesla: value of T2 texture features and geometric parameters. NMR Biomed 2012;25: 866–872.

[30] Otsu N. A threshold selection method from gray-level histograms. EEE Transactions On Systrems, Man, And Cybernetics 1979;9(1).

[31] Michopoulou S, Costaridou L, Panagiotopoulos E, Speller R, Todd-Pokropek A. Segmenting degenerated lumbar intervertebral discs from MR images. IEEE Nuclear Science Symposium Conference Record 2008.

[32] Michopoulou SK, Costaridou L, Panagiotopoulos E, Speller R, Panayiotakis G, and Todd-Pokropek A. Atlas-based segmentation of degenerated lumbar intervertebral discs from MR images of the spine. IEEE transactions on biomedical engineering 2009;56(9).

[33] Chevrefils C, Cheriet F, Aubin C, and Grimard G. Texture analysis for automatic segmentation of intervertebral disks of scoliotic spines from MR images. IEEE Transactions On Information Technology In Biomedicine 2009;13(4).

[34] Yushkevich PA, Piven J, Hazlett HC, Smith RG, Ho S, Gee JC and Gerig G. User-guided 3D active contour segmentation of anatomical structures: significantly improved efficiency and reliability. NeuroImage 2006;31:1116 – 1128.

[35] Gédet P, Thistlethwaite PA and Ferguson SJ. Minimizing errors during in vitro testing of multisegmental spine specimens: considerations for component selection and kinematic measurement. J Biomech 2007;40:1881-1885.

[36] Gédet P, Thistlethwaite PA and Ferguson SJ. Comparative biomechanical investigation of a modular dynamic lumbar stabilization system and the Dynesys system. Eur Spine J 2009;18:1504-1511.

[37] Van Rossum G and de Boer J. Interactively testing remote servers using the python programming language. CWI Q 1991;4:283–303.

[38] Smit T H, van Tunen MSLM, van der Veen AJ, Kingma I, van Dieën JH. Quantifying intervertebral disc mechanics: a new definition of the neutral zone. BMC Musculoskeletal Disorders 2011;12:38.

[39] Smit T, Odgaard A, Schneider E. Structure and function of vertebral trabecular bone.

Spine 1997;22:2823–2833.

[40] Polikeit A, Ferguson SJ, Nolte LP, Orr TE. Factors influencing stresses in the lumbar spine after the insertion of intervertebral cages: finite element analysis. Eur Spine J 2003;12:413–420.

[41] Welsch GH, Trattnig S, Paternostro-Sluga T, Bohndorf K, Goed S, Stelzeneder D, Mamisch TC. Parametric T2 and T2* mapping techniques to visualize intervertebral disc degeneration in patients with low back pain: initial results on the clinical use of 3.0 Tesla MRI. Skeletal Radiol 2011;40:543–551.

[42] Takashima H, Takebayashi T, Yoshimoto M, Terashima Y, Tsuda H, Ida K and Yamashita T. Correlation between T2 relaxation time and intervertebral disk degeneration. Skeletal Radiol 2012;41:163–167.

[43] Perry J, Haughton VM, Anderson PA, Wu Y, Fine J, Mistretta C. The value of T2 relaxation times to characterize lumbar intervertebral disks: Preliminary Results. AJNR Am J Neuroradiol 2006;27:337–342.

[44] Haughton VM, Schmidt TA, Keele K, An HS and Lim TH. Flexibility of lumbar spinal motion segments correlated to type of tears in the annulus fibrosus. J Neurosurg 2000;92:81–86.

[45] Schmidt TA, An HS, Lim, TH, Nowicki BH and Haughton VM. The stiffness of lumbar spinal motion segments with a high-intensity zone in the annulus fibrosus. Spine 1998;23:2167–2173.

[46] Peng B, Hou S, Wu W, Zhang C, Yang Y. The pathogenesis and clinical significance of a high-intensity zone (HIZ) of lumbar intervertebral disc on MR imaging in the patient with discogenic low back pain. Eur Spine J 2006;15: 583–587.

[47] Van Engelen SJPM, Ellenbroek MHM, van Royen BJ, de Boer A, van Dieën JH. Validation of vibration testing for the assessment of the mechanical properties of human lumbar motion segments. JBiomech 201;2 45:1753–1758.

[48] Gleizes V, Viguier E, Feron JM, Canivet S and Lavaste F. Effects of freezing on the biomechanics of the intervertebral disc. Surg Radiol Anat 1998;20:403-407.

[49] Tan JS and Uppuganti S. Cumulative multiple freeze-thaw cycles and testing does not affect subsequent within-day variation in intervertebral flexibility of human cadaveric lumbosacral spine. Spine 2012;37:E1238–E1242.

[50] Alini M, Eisenstein SM, Ito K, Little C, Kettler AA, Masuda K, Melrose J, Ralphs J, Stokes I, Wilke HJ. Are animal models useful for studying human disc disorders / degeneration? Eur Spine J 2008;17:2–19.

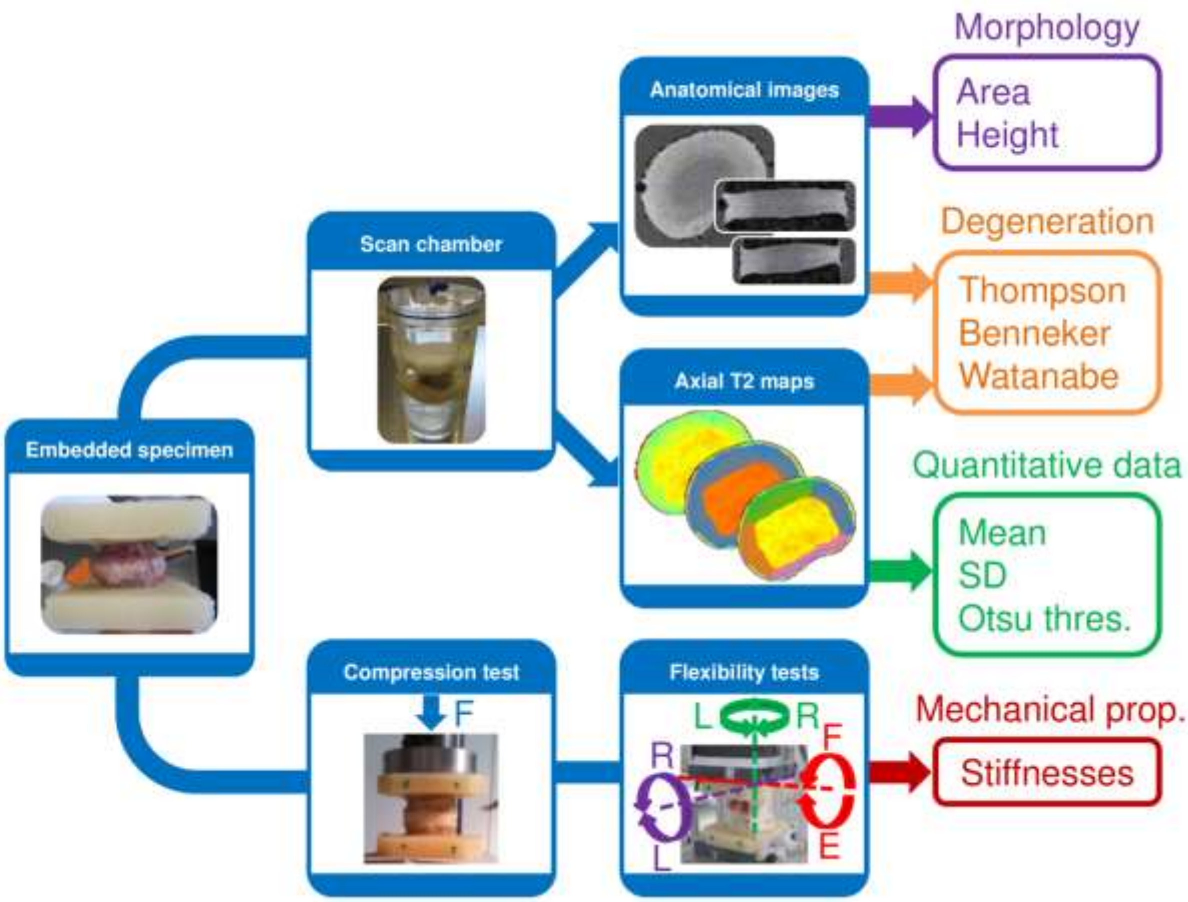

Fig. 1. Overview of the study. T_1 and T_2 weighted MRI and axial T_2 maps of 14 intervertebral segments were performed and morphological, degenerative and quantitative data were extracted or evaluated. The intervertebral stiffnesses were computed from the load-deflection curves of the tests in compression, torsion, lateral bending and flexion/extension. The relations between degenerative, quantitative and mechanical data were established.

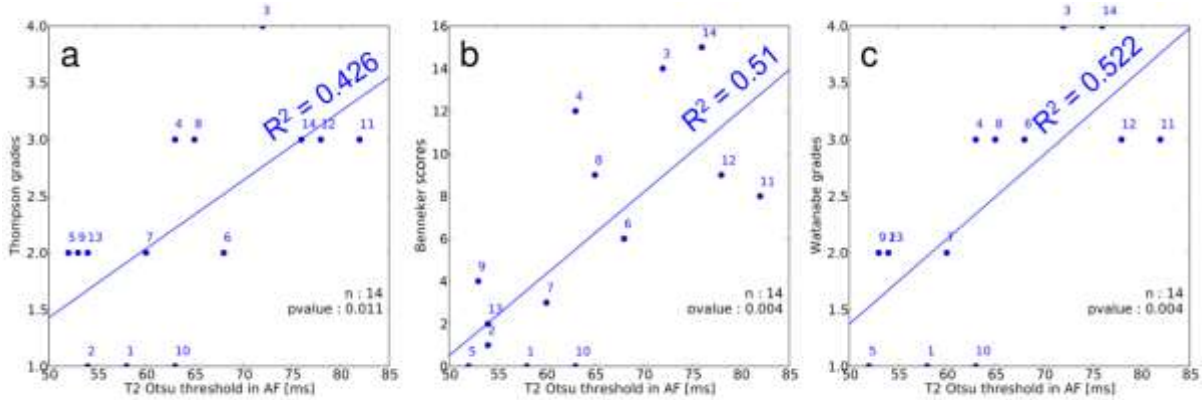

Fig. 2. Coefficient of determination (R^2) between the T_{OTSU} measured in the annulus fibrosus and Thompson (a), Benneker (b) and Watanabe (c) grading schemes. Each specimen is numbered from 1 to 14.

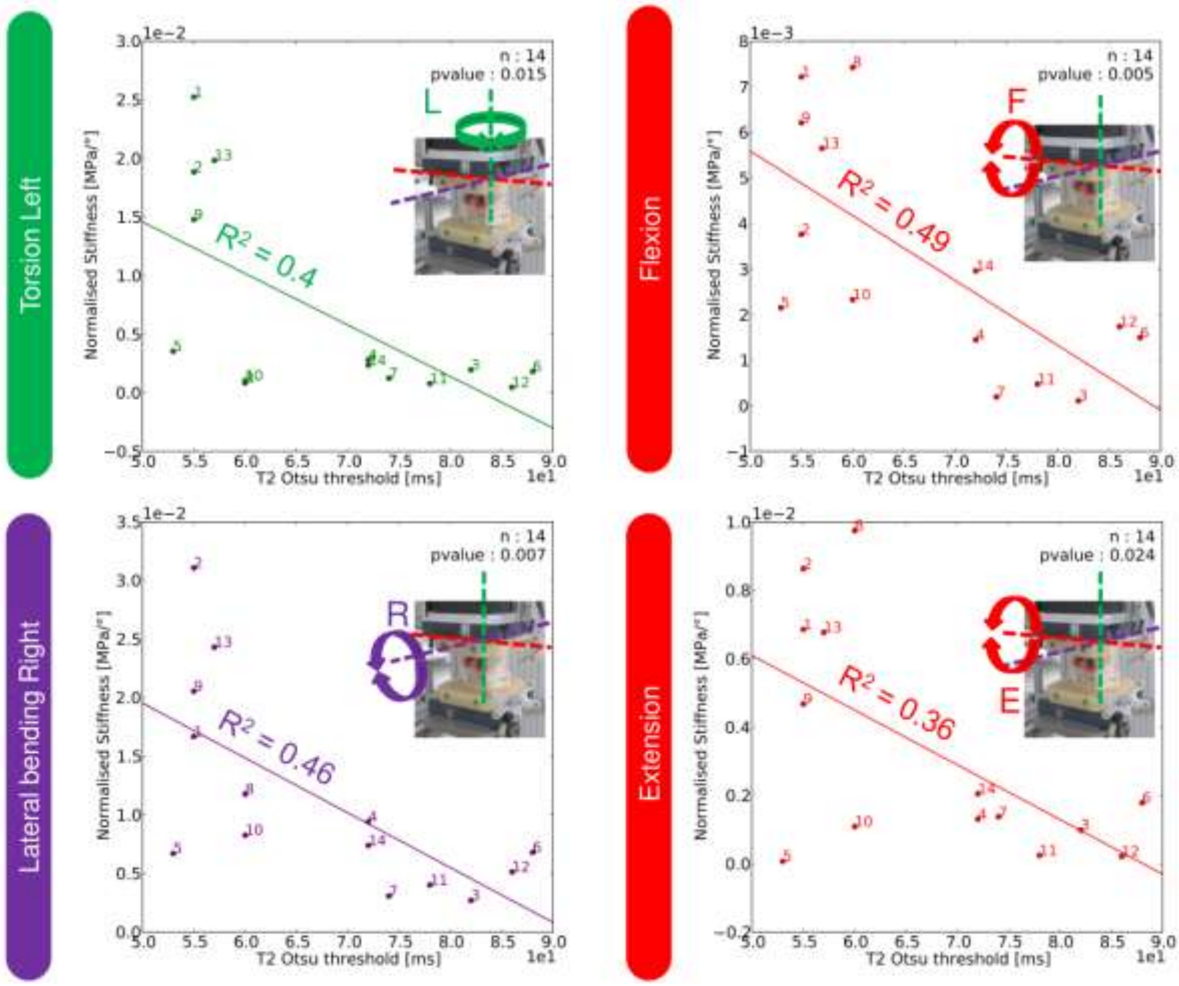

Fig. 3. Coefficient of determination (R^2) between the T_{OTSU} measured in the posterior annulus fibrosus and apparent moduli of the rotational and bending tests. Each specimen is numbered from 1 to 14.

Table 1. Consensus classification grades / scores.

	Specimen #	1	2	3	4	5	6	7	8	9	10	11	12	13	14
Thompson	Assessor 1	1	1	4	3	2	1	**2**	3	**1**	1	3	**3**	2	3
	Assessor 2	1	1	4	3	2	2	**1**	3	**2**	1	3	**4**	2	4
	Consensus	1	1	4	3	2	2	2	3	2	1	3	3	2	3
Benneker	Assessor 1	0	1	**13**	12	0	**6**	3	**8**	**1**	**1**	**8**	**8**	**2**	**15**
	Assessor 2	0	1	**14**	12	0	**3**	3	**10**	**4**	**0**	**9**	**9**	**3**	**16**
	Consensus	0	1	14	12	0	6	3	9	4	0	8	9	2	15
Watanabe	Assessor 1	1	2	**3**	3	1	**2**	**2**	**3**	**1**	1	**3**	3	2	4
	Assessor 2	1	2	**4**	3	1	**3**	**3**	**4**	**2**	1	**4**	3	2	4
	Consensus	1	2	4	3	1	3	2	3	2	1	3	3	2	4

Table 2. Coefficients of determination (R^2) computed between the degeneration grading systems, apparent moduli and values computed from the T_2 maps (mean T_2 and Otsu threshold) are represented. The significant values are bold ($p < 0.05$). Data of higher interest are highlighted in blue.

	Age	Thompson	Benneker	Watanabe	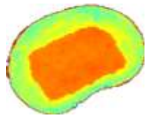 *Nucleus*		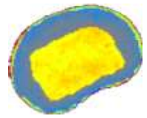 *Annulus*		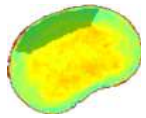 *AF Anterior*		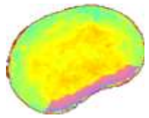 *AF Posterior*		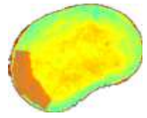 *AF Left*		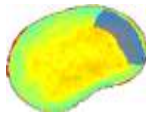 *AF Right*	
					Mean	Th.	Mean	T_{OTSU}	Mean	Th.	Mean	T_{OTSU}	Mean	T_{OTSU}	Mean	T_{OTSU}
Age	-	0,08	0,12	0,16	0,17	0,16	0,12	0,13	0,07	0,10	0,12	0,06	0,06	0,21	0,19	0,02
Thomp.	0,08	-	**0,80**	**0,73**	0,00	0,00	0,19	**0,43**	0,27	0,00	0,20	**0,37**	0,03	**0,55**	0,06	0,09
Benne.	0,12	**0,80**	-	**0,90**	0,00	0,02	0,23	**0,52**	0,27	0,03	0,21	**0,42**	0,03	**0,62**	0,14	0,15
Watan.	0,16	**0,73**	**0,90**	-	0,01	0,05	0,24	**0,52**	0,26	0,05	0,24	**0,50**	0,06	**0,52**	0,12	**0,29**
K_C	0,15	**0,36**	0,16	0,14	0,01	0,00	0,03	0,04	0,04	0,00	0,03	0,01	0,00	0,06	0,01	0,05
K_T^L	0,00	**0,35**	0,28	0,23	0,04	0,02	0,27	**0,38**	0,24	0,06	**0,38**	**0,40**	0,13	0,22	0,15	0,09
K_T^R	0,00	**0,42**	**0,33**	0,24	0,06	0,03	**0,33**	**0,46**	**0,35**	0,10	**0,38**	**0,36**	0,16	0,26	0,16	0,07
K_B^L	0,01	0,26	0,16	0,09	0,11	0,13	**0,31**	**0,42**	**0,37**	0,04	**0,32**	**0,37**	0,17	0,25	0,09	0,09
K_B^R	0,01	**0,32**	0,22	0,13	0,10	0,10	**0,30**	**0,42**	**0,33**	0,02	**0,36**	**0,46**	0,14	0,26	0,10	0,09
K_F	0,00	0,14	0,10	0,12	0,02	0,01	0,16	0,24	0,14	0,02	**0,33**	**0,49**	0,08	0,13	0,01	0,13
K_E	0,00	0,12	0,08	0,03	0,17	0,19	0,19	0,23	0,17	0,01	**0,32**	**0,36**	0,07	0,17	0,06	0,02

Table A1. Degeneration grades, T_2 maps, Mean, Standard deviation, Otsu threshold and Δ ($Mean_{nucleus}$ - $Mean_{annulus}$) computed for the specimens as well as their apparent moduli for each load case. The compressive apparent modulus is in MPa, the apparent modulus in torsion, lateral bending, flexion and extension are expressed in kPa/°. The data is organised by increasing Thompson grade.

	Scale					Quantitative T_2 data (ms)																				Apparent modulus (Comp.[Mpa], else [kPa])						
#	Thom.	Benn.	Wata.	Level	Age	Map	*Nucleus*			*Annulus*			Δ	*AF Anterior*			*AF Posterior*			*AF Left*			*AF Right*			*Comp.*	*Torsion*		*Bending*		*Flex.*	*Ext.*
							Mean	SD	Th.	Mean	SD	Th.		Mean	SD	Th.	Mean	SD	Th.	Mean	SD	Th.	Mean	SD	Th.	K_C	K_T^L	K_T^R	K_B^L	K_B^R	K_F	K_E
1	**1**	0	1	L2-L3	63	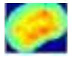	83.90	6.79	83	59.36	11.59	58	24.54	59.02	11.16	58	57.58	15.15	55	59.21	8.37	59	61.38	15.15	61	4.71	25.3	20.66	13.57	16.68	7.22	6.86
2	**1**	1	2	T12-L1	70	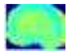	60.08	4.67	59	53.42	9.81	54	6.66	48.62	11.06	67	56.81	5.58	55	52.65	5.91	52	56.10	5.58	65	3.33	18.9	17.17	33.3	31.08	3.76	8.63
10	**1**	0	1	L2-L3	71		85.10	9.43	83	64.73	13.62	63	20.37	59.91	12.94	59	69.12	15.64	60	62.57	10.84	61	68.00	15.64	66	2	1.04	3.93	4.79	8.26	2.33	1.1
5	**2**	0	1	L4-L5	63	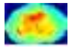	79.85	11.70	78	51.54	9.59	52	28.31	51.00	9.93	53	54.34	11.41	53	53.52	8.26	52	47.95	11.41	37	0.43	3.54	4.47	5	6.71	2.15	0.08
6	**2**	6	3	L4-L5	68	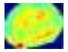	74.52	7.80	74	64.72	15.84	68	9.80	58.09	10.22	57	74.66	23.93	88	64.75	11.47	68	63.76	23.93	82	2.49	1.82	8.21	7.53	6.8	1.5	1.79
7	**2**	3	2	L2-L3	68	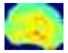	76.35	7.37	76	62.12	9.32	60	14.22	56.36	8.54	56	71.24	8.14	74	62.54	7.00	61	62.56	8.14	60	1.96	1.25	3.18	1.63	3.08	0.2	1.38
9	**2**	4	2	T12-L1	71	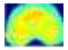	75.34	6.38	74	54.39	10.60	53	20.95	48.53	9.26	45	60.31	10.61	55	56.28	8.42	57	54.00	10.61	50	0.83	14.79	14.71	22.29	20.55	6.21	4.68
13	**2**	2	2	T12-L1	89	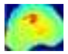	74.08	9.58	78	56.57	8.90	54	17.51	51.11	9.12	50	60.59	6.42	57	60.17	9.05	57	57.47	6.42	57	0.12	19.83	18.5	24.07	24.31	5.65	6.77
4	**3**	12	3	L4-L5	70		74.42	11.27	73	62.12	11.61	63	12.30	56.74	8.47	53	70.48	7.95	72	66.34	12.87	71	57.21	7.95	55	1.21	2.81	5.34	12.3	9.42	1.45	1.31
8	**3**	9	3	T12-L1	68	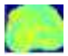	66.76	5.57	66	63.12	9.24	65	3.64	61.86	8.41	63	63.39	10.47	60	64.68	10.88	68	63.22	10.47	64	1.45	0.84	2.92	9.21	11.77	7.43	9.75
11	**3**	8	3	L4-L5	71		82.69	9.51	82	87.44	19.73	82	-4.75	89.75	29.77	86	89.05	15.67	78	84.09	9.07	82	86.21	15.67	78	0.47	0.79	1.16	1.88	4.03	0.48	0.25
12	**3**	9	3	L4-L5	89		130.65	45.55	103	75.53	20.60	78	55.12	72.46	26.66	76	84.56	14.53	86	83.53	19.74	82	74.44	14.53	74	1.94	0.46	1.53	3.54	5.13	1.74	0.22
14	**3**	15	4	L2-L3	87		72.43	9.95	74	72.30	15.33	76	0.13	71.81	13.69	75	71.02	11.76	72	82.63	17.63	81	61.78	11.76	60	0.52	2.35	2.73	5.39	7.4	2.96	2.05
3	**4**	14	4	L2-L3	70	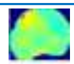	61.48	5.88	61	60.32	26.38	72	1.16	63.10	26.65	40	64.92	26.62	82	57.11	22.34	39	55.47	26.62	80	0.91	1.97	2.49	1.03	2.7	0.11	0.99